

SOLDERING HANDBOOK

3rd Edition



American Welding Society

Soldering Handbook

3rd Edition

by

Paul T. Vianco, Ph.D.

*Sandia National Laboratories,
Albuquerque, New Mexico*



American Welding Society

550 N.W. LeJeune Road, Miami, Florida 33126

Table of Contents

	Page No.
<i>Personnel</i>	<i>iii</i>
<i>Preface</i>	<i>iv</i>
<i>List of Tables</i>	<i>ix</i>
<i>List of Figures</i>	<i>xii</i>
1. Fundamentals of Soldering Technology	1
1.1 Introduction	3
1.2 Physical Metallurgy	3
1.2.1 Metals and Alloys	3
1.2.1.1 Phase Diagrams	5
1.2.1.1.1 Binary Alloy Phase Diagrams.....	5
1.2.1.1.2 Ternary Alloy Phase Diagrams	20
1.2.1.2 Structures and Properties	27
1.2.1.3 Solder Joint Formation and Microstructure.....	37
1.2.1.3.1 Wetting and Spreading of Molten Metals and Alloys (Equilibrium).....	37
1.2.1.3.2 Wetting and Spreading of Molten Metals and Alloys (Kinetics).....	56
1.2.1.3.3 Solidification and Solder Joint Metallurgy	58
1.3 Solder Joint Design for Product Manufacturability and Service Reliability.....	107
1.3.1 Product Manufacturability	107
1.3.2 Product Reliability	119
1.3.2.1 Static Loads	120
1.3.2.2 Fatigue Loads.....	125
1.3.2.3 Corrosion	132
1.3.2.3.1 Atmospheric (Environmental) Corrosion.....	134
1.3.2.3.2 Galvanic-Assisted Corrosion	135
1.3.2.3.3 Voltage-Assisted Corrosion.....	139
1.3.2.3.4 Stress Corrosion and Corrosion Fatigue Cracking.....	142
1.3.2.3.5 Corrosion Mitigation.....	142
1.4 Solder Alloy Physical Properties: Measurement Techniques	144
1.4.1 Density	144
1.4.2 Electrical Properties	145
1.4.3 Thermal Properties.....	147
1.4.3.1 Thermal Properties—DSC Analysis.....	147
1.4.3.2 Thermal Properties—DTA Analysis.....	151
1.4.4 Fluid and Solderability Properties.....	151
1.4.4.1 Fluid Properties.....	152
1.4.4.2 Wetting/Spreading and Solderability Properties.....	155
1.5 Solder Alloy and Solder Joint Mechanical Properties—Measurement Techniques	164
1.5.1 Bulk Solder Mechanical Properties Measurements	165
1.5.2 Solder Joint Mechanical Properties Measurements	165
2. Solder Materials.....	179
2.1 Introduction	179
2.2 Contamination.....	182
2.3 Specifications	187
2.4 Bulk and Joint Properties of Solder Alloys.....	188
2.4.1 Tin, Tin-Lead, Tin-Lead-Antimony, Tin-Lead-Silver, and Lead-Silver Solders.....	188
2.4.2 Tin-Antimony, Tin-Antimony-Silver (Copper), and Tin-Silver Alloys	207
2.4.3 Tin-Zinc, Zinc-Aluminum, and Other Zinc-Containing Solders	215
2.4.4 Indium, Indium-Tin, Indium-Lead, and Other Indium-Containing Solders	218
2.4.5 Bismuth-Containing (‘Fusible’) Solders.....	219

2.4.6	Au-Based Solder Alloys.....	224
2.4.7	Cd-Containing Solder Alloys.....	228
3.	Substrate Materials	229
3.1	Introduction.....	229
3.2	Coatings	230
3.3	Metallic Substrate Materials	238
3.3.1	Noble Metals and Alloys.....	241
3.3.1.1	Alloy Descriptions	241
3.3.1.2	Solder Alloys	242
3.3.1.3	Cleaning Processes and Fluxes.....	243
3.3.2	Copper and Cu-Based Alloys.....	243
3.3.2.1	Alloy Descriptions	243
3.3.2.2	Solder Alloys	248
3.3.2.3	Cleaning Processes and Fluxes.....	248
3.3.3	Steels	252
3.3.3.1	Alloy Descriptions	252
3.3.3.2	Solder Alloys	253
3.3.3.3	Cleaning Processes and Fluxes.....	253
3.3.4	Stainless Steels and High-Alloy Fe-Based Materials	254
3.3.4.1	Alloy Descriptions	254
3.3.4.2	Solder Alloys	257
3.3.4.3	Cleaning Processes and Fluxes.....	257
3.3.5	Nickel and Nickel-Based Alloys.....	258
3.3.5.1	Alloy Descriptions	258
3.3.5.2	Solder Alloys	261
3.3.5.3	Cleaning Processes and Fluxes.....	261
3.3.6	Lead.....	261
3.3.6.1	Alloy Descriptions	261
3.3.6.2	Solder Alloys	262
3.3.6.3	Cleaning Processes and Fluxes.....	262
3.3.7	Aluminum and Al Alloys.....	263
3.3.7.1	Alloy Descriptions	263
3.3.7.2	Solder Alloys	268
3.3.7.3	Cleaning Processes and Fluxes.....	269
3.3.8	Magnesium and Mg Alloys.....	275
3.3.8.1	Alloy Descriptions	275
3.3.8.2	Solder Alloys	277
3.3.8.3	Cleaning Processes and Fluxes.....	279
3.3.9	Tin and Sn Alloys.....	280
3.3.9.1	Alloy Descriptions	280
3.3.9.2	Solder Alloys	281
3.3.9.3	Cleaning Processes and Fluxes.....	281
3.3.10	Zinc and Zn Alloys	281
3.3.10.1	Alloy Descriptions	281
3.3.10.2	Solder Alloys	282
3.3.10.3	Cleaning Processes and Fluxes.....	282
3.3.11	Refractory Metals and Alloys	283
3.3.11.1	Alloy Descriptions	283
3.3.11.2	Solder Alloys	283
3.3.11.3	Cleaning Processes and Fluxes.....	283
3.3.12	Special Materials—Electrical Contact Materials	284
3.3.12.1	Alloy Descriptions	284
3.3.12.2	Solder Alloys	285
3.3.12.3	Cleaning Processes and Fluxes.....	285

3.4	Nonmetallic Materials.....	286
3.4.1	Ceramics and Glasses.....	286
3.4.1.1	Material Description	286
3.4.2	Solder Alloys.....	288
3.4.3	Cleaning Processes and Fluxes	288
4.	Fluxes	291
4.1	Introduction.....	291
4.1.1	Fundamental Concepts.....	291
4.1.2	How to Use a Flux.....	294
4.1.3	Flux Types.....	295
4.1.3.1	Rosin-Based Fluxes	297
4.1.3.2	Organic Acid Fluxes	300
4.1.3.3	Inorganic Acid Fluxes.....	301
4.1.3.4	Reaction Fluxes	301
4.1.3.5	Atmospheres	304
4.1.3.5.1	Inert Atmospheres and Vacuum	304
4.1.3.5.2	Reactive Atmospheres.....	309
5.	Solder Pastes.....	311
6.	Assembly Processes.....	313
6.1	Introduction.....	313
6.2	Incoming Material Storage and Handling.....	313
6.3	Preassembly Preparation (Precogning) Processes	315
6.4	Soldering Processes.....	319
6.4.1	Introduction.....	319
6.4.1.1	A ‘Global’ Perspective.....	319
6.4.1.2	Process Development Logistics	319
6.4.2	Hand Soldering	323
6.4.2.1	Soldering Iron	324
6.4.2.2	Soldering with a Torch (Flame).....	333
6.4.2.3	Process Development—General Remarks.....	345
6.4.3	Semiautomated and Automated Soldering.....	348
6.4.3.1	Variations on Torch Soldering (Robotic Automation).....	348
6.4.3.2	Furnace Soldering	349
6.4.3.2.1	Apparatus	349
6.4.3.2.2	Process Development	354
6.4.3.3	Vapor Phase Soldering	385
6.4.3.4	Immersion (Dip) Soldering.....	388
6.4.3.5	Induction Soldering	406
6.4.3.6	Resistance Soldering.....	418
6.4.3.7	Laser Beam Soldering	423
6.4.3.8	Hot Gas Soldering	427
6.4.3.9	Ultrasonic Soldering	428
6.5	Postassembly Cleaning Techniques	435
6.5.1	Solder Assembly Residues.....	435
6.5.2	Cleaning Techniques	436
6.5.3	Verification Techniques.....	443
6.6	Storage Considerations	444
7.	Inspection Techniques for Product Acceptance and Process Optimization	447
7.1	Introduction.....	447
7.2	Defects	447
7.3	Quantitative Defect Analysis	452
7.4	Defect Detection	454

7.4.1	Nondestructive Techniques	455
7.4.1.1	Visual Inspection and Microscopy.....	456
7.4.1.2	X-ray Radiography/Laminography.....	458
7.4.1.3	Ultrasonic Inspection	461
7.4.1.4	Infrared (or Dynamic Thermal) Imaging.....	465
7.4.1.5	Pressure and Vacuum Leak Testing	468
7.4.1.6	Proof Testing.....	470
7.4.1.7	Liquid Dye or Fluorescent Dye Penetrant	471
7.4.2	Destructive Techniques	472
7.4.2.1	Metallographic Cross-Sectioning	472
7.4.2.2	Mechanical Testing.....	484
7.5	Rework and Repair.....	489
8.	Environmental, Safety, and Health	501
8.1	Introduction.....	501
8.2	Base Metals.....	503
8.3	Fluxes	504
8.4	Solders.....	505
8.5	Soldering Processes.....	508
8.6	Cleaning Processes.....	509
Annexes		
A	Solution of the Thermal Expansion Mismatch Equations for a Two-Base Material System (Single Joint) Having Isotropic Materials and Temperature-Independent Material Properties.....	513
B	Metallographic Sample Preparation Procedure for Soft Solder Joint Specimens	516
B.1	Grinding and Polishing Procedure	516
B.2	Etchant for Intermetallic Compound Layer Accent—Cu Substrate.....	516
C	Microstructures of Commonly Used Solder Alloys	517
D	Use of Thermocouples to Monitor Part Temperatures	526
E	References	531
	Index	541

List of Tables

Table	Page No.
1.1 Table of the Elements, Giving Symbol, Atomic Number, and Atomic Mass	8
1.2 <i>D</i> Parameters vs. the d_m/H (r/H) Parameter for the Koshevnik et al., Calculation of the Solder/Flux Interfacial Tension γ_{LF}	49
1.3 Solderability Parameters of θ_c , γ_{LF} and $\gamma_{SF}-\gamma_{SL}$ Measured by the Wilhemy Plate (Wetting Balance) Configuration for a Variety of Substrate Materials, Solder Compositions, and Fluxes	51
1.4 Thermal Expansion Coefficients of Materials Commonly Encountered in Soldering Technology	72
1.5 Solid-State Growth Kinetics Parameters for Selected Solders on Cu Substrate	91
1.6 Intermetallic Compound Layer Thickness on Soft and Hard Cu as a Function of Solder Alloy for Extended Aging Times (<15 Years)	92
1.7 Solid-State Intermetallic Compound Layer Growth Kinetics for Sn and Sn-Pb Solder Coatings on 70Cu-30Zn (Half-Hard) Cartridge Brass	98
1.8 Solid-State Growth Kinetics Parameters for Selected Solder and Substrate Combinations	100
1.9 Temperature-Dependent Values of the Shear Modulus, G , the Shear Yield Stress, γ_y , and the Shear Yield Strain, γ_e , for 63Sn-37Pb Solder	131
1.10 Standard Reduction Potentials (SRP)	138
1.11 Density, Electrical Conductivity, Thermal Conductivity, and Coefficient of Thermal Expansion for Sn-Pb Alloys and Several Other Solders	146
1.12 Viscosity Data for Selected Metals and Alloys	154
1.13 Viscosity Data for Sn-Pb Alloys at Specific Temperatures.....	155
1.14 Qualitative Description of Base Metal Wettabilities.....	157
1.15 Guidelines and Specifications for Solderability Testing for Electronics Applications.....	157
1.16 List of ASTM Test Methods and Practices for Evaluating the Mechanical Properties of Bulk Materials	166
1.17 List of ASTM Test Methods and Practices for Evaluation of the Mechanical Properties of Adhesive Joints	167
2.1 Forms of Solder Materials.....	179
2.2 Resistivities of Common Metal Elements.....	182
2.3 Impurity Limits for Virgin Solder (ASTM B32) and Maximum Concentrations in Working Sn-Pb Solder Baths (IPC-S-815A).....	184
2.4 ASTM B339 Grades, Purity Levels, and Uses of Sn	189
2.5 Physical Properties of Sn	190
2.6 Tensile Properties of Sn	191
2.7 Creep Properties of Sn	192
2.8 Impact Properties of Sn.....	192
2.9 Shear Strength of Cu Ring-and-Plug Tests with 100Sn Joints as a Function of Test Temperature and Test Speed.....	192
2.10 Stress to Rupture Data for Cu Ring-and-Plug Tests with 100Sn Joints as a Function of Stress and Temperature.....	192
2.11 Cyclic Compression/Tension Fatigue Life Data for Cu Ring-and-Plug Test with 100Sn Joints as a Function of Maximum Stress and Temperature	192
2.12 ASTM B32 Specification for Sn-Pb, Sn-Pb-Sb, Sn-Pb-Ag, and Pb-Ag Solders	193
2.13 ISO/DIS 9453 Specification for Sn-Pb, Sn-Pb-Sb, Sn-Pb-Ag, and Pb-Ag Solders.....	194
2.14 Composition Limits and Applications for Pb	195
2.15 Physical Properties of Pb	196
2.16 Bulk Mechanical Properties of Sn-Pb Solders	197
2.17 Bulk Tensile Strength Properties of 60Sn-40Pb Solder as a Function of Test Temperature and Testing Rate.....	197
2.18 The 0.2% Offset Yield Strength Data of Sn-Pb Alloys.....	198
2.19 Mechanical Properties of Sn-Pb Solders at Low Temperatures.....	198

2.20	Creep Life Data for Bulk Sn-Pb and Sn-Pb-Sb Alloys	200
2.21	Room-Temperature Tensile Strength of Cu Butt Joints Formed with Sn-Pb Solders, as a Function of Tin Content	200
2.22	Torsional Shear Test Strengths of Cu Soldered Joints	200
2.23	Rated Internal Pressure for Cu Tube Solder Joints	201
2.24	Physical Properties of 60Sn-40Pb Alloy	201
2.25	Solderability Parameters of Contact Angle (θ_c) and Solder-Flux Interfacial Tension (γ_{LF}) for 60Sn-40Pb and 63Sn-37Pb Solders	202
2.26	Creep Rupture Strength of Bulk 60Sn-40Pb Solder	203
2.27	Ring-and-Plug and Simple Lap Shear 60Sn-40Pb/Cu Solder Joint Strengths as a Function of Test Temperature and Testing Rate	205
2.28	Ring-and-Plug Creep Rupture Data for 60Sn-40Pb/Cu Solder Joints as a Function of Temperature and Stress	206
2.29	Ring-and-Plug Fatigue Life Data for 60Sn-40Pb/Cu Solder Joints as a Function of Applied Stress, Test Temperature, and Displacement Rate	207
2.30	Corrosion of Solders and Zn in Seawater	208
2.31	Corrosion Data for Pb and Sn in Various Media.....	209
2.32	Mechanical Properties of Sn-Pb-Sb Solders	211
2.33	Room-Temperature Ultimate Tensile Strength and 0.2% Offset Yield Strength Data for Several Sn-Pb-Ag Solders.....	211
2.34	ASTM B32 Solder Compositions for Sn-Sb and Sn-Ag-Sb-Cu Alloys	212
2.35	ISO/DIS Solder Specification for the 95Sn-5Sb Alloy.....	212
2.36	Physical Properties of the 95Sn-5Sb Solder	212
2.37	Alloy 95Sn-5Sb Bulk Tensile Strength and Ring-and-Plug Shear Strength as a Function of Testing Rate and Temperature	213
2.38	Alloy 95Sn-5Sb Bulk Creep Rupture Data	213
2.39	Alloy 95Sn-5Sb Ring-and-Plug Creep Rupture (Shear) Data.....	214
2.40	Alloy 95Sn-5Sb Ring-and-Plug Fatigue Strength (Shear) Data	214
2.41	Alloy 96.5Sn-3.5Ag Bulk Tensile Strength and Ring-and-Plug Shear Strength Data as a Function of Testing Rate and Temperature	215
2.42	Alloy 96.5Sn-3.5Ag Ring-and-Plug Fatigue Data as a Function of Testing Rate	216
2.43	Shear Stress at Failure of Double Cantilever Beam, Al Shear Samples Made with Sn-Zn Solders.....	216
2.44	Shear Stress at Failure of Double Cantilever Beam, Al Shear Samples Made with 96Sn-4Zn Solder, as a Function of Solder Joint Gap Thickness.....	216
2.45a	ANSI/J-STD-006 and ISO/DIS 9453 Specifications Covering the In-Containing Solders	219
2.45b	Chemical Compositions of Soft Solder Alloys Other Than Tin-Lead and Tin-Lead-Antimony Alloys ...	219
2.46	Properties of Bulk In-Containing Solders.....	220
2.47	Properties of Bulk In-Pb and In-Sn Solders.....	220
2.48	Shear Strength of 58In-42Sn/Cu Joints as a Function of Test Temperature and Strain Rate.....	220
2.49	ASTM B 32, ISO/DIS 9453, and ANSI/J-STD-006 Specification Covering the Bi-Based, and Bi-Containing Solders.....	222
2.50	Some Properties of Low Melting Solders Containing Bi.....	223
2.51	Shear Strength (as a Function of Test Temperature and Crosshead Speed), Creep Rupture Strength, and Fatigue Resistance of Cu Ring-and-Plug Samples Made with the 58Bi-42Sn Solder.....	224
2.52	ANSI/J-STD-006 Specification for Compositions of the Eutectic Au-Sn, Au-Ge, and Au-Si Solders.....	226
2.53	Young's Modulus (Elastic Modulus) and Thermal Expansion Coefficient as a Function of Temperature for Bulk Au-Ge, Au-Sn, and Au-Si Eutectic Bonding Materials	226
3.1	Tin and Solder Coating Protective Finishes per MIL-STD-1276D	231
3.2	Solderable and Protective Finishes for Selected Difficult-to-Solder Substrate Materials, Based Largely Upon MIL-STD-1276D	234
3.3	Table of Noble Metals and Alloys and Their Melting Properties	242
3.4	General Description of Common Wrought and Cast Cu Alloys.....	244

3.5	Stress Relieving Temperature for Wrought Cu Alloys	245
3.6	Precleaning Solutions for Cu and Cu Alloys	249
3.7	Solderability Ranking and Flux Requirements of Cu and Cu-Alloys.....	251
3.8	General, Inorganic Fluxes for Use on Cu and Cu-Based Alloys	252
3.9	AISI Nomenclature for Low-Carbon and Low-Alloy Steels	258
3.10	Inorganic Fluxes for Steels, Stainless Steels, Monel Alloy, Cast Fe, and Al Alloys	252
3.11	List of Commonly Used Stainless Steels	256
3.12	List of Cleaning Chemistries for Stainless Steels	258
3.13	List of Commonly Used Ni-Based Alloys	260
3.14	List of Etching and Electropolishing Solutions for Tarnish Removal of Pb and Pb-Alloys	262
3.15	List of Commonly Used Al-Based Alloys	263
3.16	Qualitative Comparison of the Corrosion Potential of Dissimilar Metal Joints Containing Al or Al Alloys.....	265
3.17	Heat Treat Temperatures and Times to Realize <i>Full Anneal</i> or “O” Temper in Wrought Al Alloys	266
3.18	Etchants for Al and Al-Based Alloys for Potential Scale-up as Precleaning Processes	270
3.19	List of Commonly Used Mg-Based Alloys.....	276
3.20	Maximum Time at Temperature for Exposure of Mg Alloys Before Significant Changes Take Place to the Alloy Properties	277
3.21	Candidate Solder Alloys for Use on Mg and Mg-Based Alloys.....	279
3.22	List of the Refractory Metals and Their Melting Temperatures	283
3.23	Cleaning Techniques for Refractory Metals	284
3.24	Softening Temperatures of Common Glasses and Plastics.....	287
4.1	List of Flux Designations as Provided in ANSI/J-STD-004.....	297
4.2	List of Documents Related to Solder Flux Testing	298
4.3	List of ASTM and ISO Documents for Solder Flux Testing	298
4.4	List of ISO, ASTM, and ANSI/J-STD Specifications on Solder Pastes and Flux Core Solder Wire.....	298
4.5	List of Inorganic Acid Fluxes and Metal Systems for Which Each Flux Is Most Effective	302
4.6	The Proportions of N ₂ , O ₂ , Ar, and CO ₂ Contents in Air, as Expressed in vol.%, wt.%, Parts-Per-Million (ppm), and Partial Pressure	305
5.1	Solder Paste Properties for Screen Printing, Stencil Printing, and Dispensing Techniques	312
6.1	General Guide to Solder Iron Power Rating and Tip Size	327
6.2	Properties of Common Fuel Gases.....	336
6.3	Emissivities of Common Metal Surfaces.....	352
6.4	Dew Point Temperatures Expressed as Moisture Content	356
6.5	Materials/Process Step Matrix	363
6.6	Contamination Levels Based Upon Material Procurement (ASTM B32) and Solder Process Baths (IPC-S-815A).....	396
6.7	Computed Penetration Depths as a Function of Induction Field Frequency	411
6.8	Electrical Resistivity, $c_p\gamma$, and Thermal Conductivity as a Function of Temperature for Selected Materials	415
7.1	Leak Rate Specifications.....	469
8.1	TWA Standards for Several Elemental Metals.....	506
8.2	Airborne Pb Concentrations for Typical Soldering Processes	507

List of Figures

Figure	Page No.
1.1	Historical time line of soldering technology 2
1.2	The material consistency of an alloy undergoing solidification which does take place over the temperature range $T_s < T < T_l$ 4
1.3	The binary Sn-Pb alloy system phase diagram 6
1.4	Sn-Pb alloy phase diagram to illustrate text discussion on 85Sn-15Pb 9
1.5	Optical micrograph of the microstructure of the 85Sn-15Pb solder. The dark areas are the Pb-rich phase; the light regions are the Sn-rich phase. The cooling rate was 10°C/18°F/min 10
1.6	Optical micrograph of 63Sn-37Pb solder microstructure following aging at 70°C/158°F for 400 days in order to realize an equilibrium condition 10
1.7	Sn-Pb Alloy phase diagram to illustrate the text discussion on the 95Pb-5Sn starting composition..... 11
1.8	Optical micrograph of the microstructure of the 95Pb-5Sn solder. The cooling rate was 10°C/18°F/min 12
1.9	Binary alloy phase diagram for the Cu-Sn system..... 13
1.10	Binary alloy phase diagram for the Au-Sn system..... 13
1.11	Binary alloy phase diagram for the Ni-Sn system 14
1.12	Binary alloy phase diagram of the Cu-Sn system with instructive markers per the text 14
1.13	Reaction product development at solder/substrate interfaces through the use of the binary alloy phase diagrams: (a) Schematic diagram of phase identification in bimetal couples for a simple (AB) eutectic diagram. (b) Optical micrograph of the interface region between molten 100Sn and Cu after 300 s at 260°C (500°F). (c) Optical micrograph of the molten Sn/Cu interface after 300 s at 340°C (644°F). (d) Interfacial layer development from solid-state aging at 170°C (338°F) for 402 days 16
1.14	Binary alloy phase diagram of the Au-Ag system 17
1.15	Binary alloy phase diagram of the Au-Ni system 18
1.16	Binary alloy phase diagram of the In-Sn system 19
1.17	A “first cut” of a three-dimensional, ternary alloy phase diagram. The graph of the axes is shown in (a). The horizontal axes are A and B; the vertical axis is temperature. The example of a solid solution alloy AB is illustrated in (b)..... 20
1.18	Construction of the Gibbs triangle for the ternary alloy comprised of A, B, and C. (a) Outline with each component at the apex of the equilateral construct. (b) The triangle with the lines of constant A component (as fractional quantity) in place. (c) The fully constructed Gibbs triangle for the A-B-C ternary system 21
1.19	(a) Three-dimensional phase diagram (Gibbs triangle) for a simple solid-solution alloy. (b) Isothermal section through the phase diagram entirely in the solid solution phase α . (c) Isothermal section through the liquidus and solidus surfaces. (d) Isothermal section through the liquidus and solidus surfaces, but at a higher temperature than in (c)..... 23
1.20	Liquidus projection map for a solid-solution alloy 24
1.21	Ternary alloy phase diagrams for the Ag-Bi-Pb system: (a) Liquidus projection. (b) Three-dimensional schematic view to illustrate the liquidus trough. (c) The isothermal section at 127°C (261°F)..... 25
1.22	Isopleth sections through simple solid-solution ternary phase diagram: (a) B varies from 0% to 100% while the ratio of A to C remains fixed; (b) two-dimensional construction of (a); (c) A is fixed while B and C are allowed to vary; and (d) the two-dimensional construction of the case in (c) 26
1.23	The pseudo-binary alloy phase diagram (isopleth) for the ternary Au-Sn-Pb system, for the case of constant 63Sn-37Pb ratio and variable Au content 27
1.24	(a) Schematic of the dislocation, looking down its “core”; (b) Transmission electron micrograph of dislocations in “half hard” α -brass. (c) Movement of a dislocation and resulting displacement of material under an applied stress σ 29
1.25	(a) Face-centered cubic (FCC) crystal structure. (b) Hexagonal close-packed (HCP) crystal structure. (c) Body-centered cubic (BCC) crystal structure. (d) Body-centered tetragonal (BCT) crystal structure..... 29

1.26	(a) Optical micrograph of the 63Sn-37Pb solder showing the Pb-rich (dark) and Sn-rich (light) phases along with the grains of the latter phase after low-temperature aging at 70°C for 350 days. (b) Frequency bar charts for the Pb-rich particle distribution shown in (a)	31
1.27	Optical micrograph of the microstructure of the 96.5Sn-3.5Ag solder, showing the Sn-rich phase and Ag-rich Ag ₃ Sn phase particles	32
1.28	Schematic representation of the microstructural features observed in a two-phase material such as found in a number of solder alloys. Within each of the phases, there can also exist a grain structure pertinent to that material	32
1.29	(a) Grain boundary sliding in a 98.14Sn-3.33Ag-4.83Bi ternary solder subjected to thermal cycling. (b) Phase boundary sliding in 58Bi-42Sn near-eutectic solder subjected to thermal cycling. (c) Material discontinuities in the form of voids and cracks as they form by the three deformation mechanisms of dislocation motion. Optical micrographs are provided which illustrate the latter two cases	33
1.30	Optical micrograph of the 58Bi-42Sn solder. The darker phase is Bi-rich; the lighter phase is Sn-rich.....	35
1.31	Optical micrograph of a 58Bi-42Sn solder joint between Cu and an organic laminate substrate that was exposed to a thermal cycling environment of: 0°C to 100°C (32°F to 212°F), 10°C/min (18°F/min), 5 min hold at the limits, and 2500 cycles	35
1.32	TEM photographs of dislocation tangles in (a) 1100 Al (mild) and (b) ANSI Type 304 stainless steel (severe) following strain hardening caused by cold working.....	36
1.33	(a) Optical micrograph cross section and (b) SEM stereo micrograph of the through-hole solder joint of a resistor lead. (c, d) The solder joint on a surface mount resistor. These cases represent electronics applications	38
1.34	The strength properties of the solder joint components: (1) substrate(s), (2) solder strength, and (3) the strength of the interfaces between the solder and the substrate(s) determine the overall performance of the joint.....	39
1.35	Schematic representation of solder wetting and solder spreading. (a) The solid solder is placed on the substrate. (b) The molten solder has wet the substrate, but has not spread beyond its initial footprint. (c) The molten solder has wet <i>and</i> spread on the substrate surface.....	40
1.36	Schematic representation of solder (molten) spreading: (a) On open surfaces. (b) By the process of capillary flow in confined geometries (e.g., a gap).....	41
1.37	Schematic diagrams of open surface solder spreading for: (a) the formation of a sessile drop on a horizontal surface and (b) the formation of a meniscus on a vertical surface. The parameter, θ_c , is the <i>contact angle</i>	42
1.38	Schematic diagrams of the open surface solder spreading configuration, including the presence of a flux coating as would be the case in actual applications: (a) Spreading on an infinite, horizontal surface. (b) The meniscus rise on a vertical surface to a height, H	42
1.39	Schematic diagram of the solder wetting profile on a horizontal surface showing the cases of: (a) Wetting. (b) Nonwetting. (c) Dewetting. Photographs of the corresponding phenomena, looking down on the surface, appear below each profile	44
1.40	Formation of the Cu ₃ Sn and Cu ₆ Sn ₅ intermetallic compound (sub-) layers at the interface between Cu and 63Sn-37Pb solder and accentuated by thermal aging.....	45
1.41	Schematic diagram of dewetting resulting from the presence of nonwetable patches on the substrate surface. A thick, molten solder film is able to bridge those nonwetable areas; however, such is not the case when the solder coating thins out, resulting in dewetting	45
1.42	Schematic diagram of dewetting caused by the formation of a reaction product at the solder/ substrate interface during contact between the molten solder and the base material. Should the reaction product have poor wettability, its growth can reach a critical extent, resulting in dewetting of the solder film, particularly when the latter is very thin	46
1.43	Schematic diagram illustrating dewetting that results from the dissolution of a solderable coating placed over a difficult-to-solder or unsolderable base material surface.....	47
1.44	Schematic diagram of the dissolution processes occurring during the wetting and spreading of a solder film over a Au-Ni finish. The wetting and spreading of solder over the Au film is followed by the Au coating being dissolved into the solder; the solder then wets the underlying Ni coating surface. A limited amount of dissolution of the Ni layer also takes place.....	47

1.45	Schematic diagrams of a sessile drop on an infinitely wide surface. Cases (a) and (b) assume the spherical cap geometry for wetting and non-wetting, respectively. Case (c) is the case of wetting, but to an extent that the spherical cap geometry configuration can no longer be assumed	48
1.46	Contact angle as a function of the observed meniscus rise for a range of wire radii. These data are based upon a solder interfacial tension of 400 dynes/cm (close to the value for molten 63Sn-37Pb solder) and a solder density of 8 g/cm ³	51
1.47	Solder fillet profile at (a) the corner between two flat plates and (b) between a vertical wire (0.6 mm, 0.024 in.) and a flat plate	52
1.48	Schematic diagram of the solder fillet formed between two flat plates. The top and bottom surfaces are connected via the joint gap. Adding solder to the top side increases the size of the fillet until a critical solder quantity is reached. Adding solder beyond that point (“super-critical”) does not increase fillet sizes, but simply causes the additional alloy to drip down from the joint	53
1.49	Substrate orientation and geometries for which gravity has a significant effect on soldering of the joint	53
1.50	Capillary rise (h) of a fluid up a tube having a circular cross section or radius, r	54
1.51	Schematic diagram of the three basic configurations described by the kinetics, or rate, of solder wetting and spreading: (a) Sessile drop spreading on a horizontal surface. (b) Capillary rise in a vertical tube. (c) Capillary flow down into a horizontal tube or gap.....	57
1.52	Optical micrographs of the cylindrical solder joint (in cross section) between 96.5Sn-3.5Ag solder and Cu exemplifying the presence of voids and the range of their sizes. Voids can be very large so as to (a) span the entire gap thickness, or (b) be very small.....	59
1.53	Scanning electron micrographs of a solder joint formed with a Sn-Cu-Ag solder, showing the presence of several “blow holes” on the fillet surface. These defects are shown in (a) low magnification and (b) at higher magnification.....	59
1.54	Schematic diagrams of: (a) The blind gap and blind hole, solder joint geometries. (b) Measures to allow trapped flux, volatiles and air to escape from the gap hole.....	60
1.55	(a) Round voids characteristic of entrapped gases such as flux volatiles and air. (b) Optical micrograph of a solder joint showing the presence of voids due to entrapped gases. (c) Optical micrograph illustrating that small voids due to entrapped gas that may cling to the solder/substrate interface. (d) Schematic diagram of voids formed as a result of nonwetting on the substrate surface. (e) Optical micrograph exemplifying a nonwetting void, in this case due to a loss of the solderable Ni layer that exposed the underlying metallized (unsolderable) ceramic substrate	62
1.56	Schematic diagram of voids in a solder joint: (a) Large voids, but few in number. (b) A large number of relatively small voids. The footprint view looks down on the joint; the profile view looks at section AA'.....	63
1.57	(a–c) Schematic diagram of the precipitation of low melting temperature phases on the grain boundaries (or phase boundaries) in a solidification event. (d) Significant concentration of precipitated phases at the grain boundary can provide an easy path for crack propagation, thus lowering the solder (and joint) strength	65
1.58	Phase diagram segment to illustrate compositional variations due to nonequilibrium solidification.....	66
1.59	Schematic diagram of the solidification process of a binary (isomorphous) alloy under nonequilibrium conditions corresponding to the phase diagram segment in Figure 1.58. Diffusion processes in the liquid phase are infinitely fast; those in the solder phase are slow. (a) The start of solidification at T ₁ : Liquid phase has composition L ₁ and the solid precipitates with composition α ₁ . (b) Temperature T ₂ : Liquid phase composition, L ₂ , and solid-state phase composition of α ₂ ' resulting from the combination of layer compositions: α ₁ + α ₂ . (c) Temperature T ₃ : Liquid phase composition, L ₃ , and solid-state phase composition of α ₃ ' resulting from the combination of layer compositions: α ₁ + α ₂ + α ₃ . (d) Temperature T ₄ (complete solidification if the system were at equilibrium) Liquid phase composition, L ₄ , and solid-state phase composition of α ₄ ' resulting from the combination of layer composition α ₁ + α ₂ + α ₃ + α ₄ . (e) Temperature T ₅ : (complete solidification of the nonequilibrium system) Solid-state phase composition of α ₅ ' resulting from particles of the combined layer composition α ₁ + α ₂ + α ₃ + α ₄ + α ₅ , as the remaining liquid of composition, L ₅ , precipitates out of α ₅	67
1.60	Optical micrographs of the solidification structure of a 95.57Sn-3.47Ag-0.96Bi alloy under: (a) Low magnification. (b) High magnification	68

1.61	Scanning electron micrographs of solidification voids in a Sn-Cu-Ag solder joint at: (a) Low magnification. (b) A void at high magnification. (c) Optical micrograph of a cross sectional view showing the solidification void in a solder fillet profile	69
1.62	Optical micrographs of electronic solder joints exemplifying solidification cracking (a) in 96.5Sn-3.5Ag solder and (b) at the solder/substrate interface (more common location). The solder alloy in (b) is 91.84Sn-3.33Ag-4.83Bi.....	69
1.63	(a) Schematic diagram of the geometry changes to dissimilar materials upon cooling and their effects on the solder joint representing the case of global thermal expansion mismatch. The thermal expansion coefficient of base material #1 (α_1) is greater than that of base material #2 (α_2). (b) Schematic diagram of the geometry changes to the solder joint formed between similar substrate materials as would be the case of local thermal expansion mismatches. The thermal expansion coefficient of the solder (α_3) is greater than that of the base materials. In both cases (a) and (b), locally higher residual stresses will develop at the corners (arrows)	71
1.64	Schematic diagram of the formation of residual stresses in dissimilar materials that would be attached by a solder joint. It is assumed in this example that the solder joint behavior has a negligible role: (a) Both bars have the same length l_0 and are at the same temperature T_0 . (b) Unconstrained contraction of A and B as the temperature drops to T_f . (c) The constrained contraction of materials A and B with a solder joint. (d) The resulting geometry of the joined A and B materials as constrained by the presence of the solder joint.....	73
1.65	Schematic diagram of the a solder joint for analytical computation of the global, thermal expansion mismatch residual stresses: α_i is the layer thickness; E_i is the layer elastic modulus; α_i is the layer thermal expansion coefficient; and ν_i is the layer Poisson's ratio.....	74
1.66	Schematic diagram of potential residual stresses that form in cylinder-shaped joints upon cooling after solidification. The type of stress (tensile versus compressive) depends upon the relative magnitudes of the thermal expansion coefficient of the base materials (and solder). The specific mechanical properties and geometries of the substrates and solder will also affect the magnitude of the respective residual stresses.....	76
1.67	Schematic diagram of the a solder joint that illustrates each of the components: (a) "standard" configuration in which solder directly wets the base metal and (b) the case in which a solderable finish is present over the substrate material	78
1.68	Dissolution rates of base metal wires into 60Sn-40Pb solder as a function of (molten) solder temperature....	78
1.69	Dissolution rates of Cu wire as a function Sn content in Sn-Pb and Sn-Pb-Ag solders for several molten solder temperatures. The temperature scale appears at the top of the plot	79
1.70	Dissolution of Cu base metal after exposure to molten 100Sn at 300°C (572°F) for 60 s	79
1.71	(a) Cu_6Sn_5 precipitates from Cu dissolved into molten 100Sn during hot solder dipping. (b) The needles may also be observed to grow from the interface as for the case of a Sn-Ag-Bi solder on Cu	80
1.72	(a) Needles of AuSn_4 intermetallic compound that precipitated from Au dissolved in 63Sn-37Pb solder. (b) IZOD impact strength as a function of Au concentration in 63Sn-37Pb solder showing the defect of "Au embrittlement".....	81
1.73	Schematic diagram of a hypothetical, binary alloy phase diagram between elements A and B and the potential microstructure that forms at the interface of the A-B diffusion couple at a temperature of T_i (solid-state)	82
1.74	(a) Reproduction of the Cu-Sn binary alloy phase diagram. (b) Interface microstructure between 100Sn and Cu that has been (solid-state) aged at 135°C for 350 days showing the ϵ (Cu_3Sn) and η' (Cu_6Sn_5) intermetallic (sub)layers	83
1.75	Ratio of ϵ (Cu_3Sn) to the intermetallic compound layer thickness for the (a) 100Sn/Cu couple and (b) 63Sn-37Pb/Cu couple	84
1.76	Schematic diagram of the grazing angle technique to modify the interface microstructure of solder joints. The actual thickness, h , is amplified to an effective value H by the factor, $1/\cos\theta$	85
1.77	Schematic diagram of the commonly used methodology for plotting intermetallic compound layer thickness as a function of aging time and temperature: (a) Thickness vs. time with curves pertaining to each temperature. (b) $\ln(y - y_0)$ vs. $\ln(t)$ for each test temperature	87

1.78	Graph of $\ln(y - y_0)$ versus $\ln(t)$ for the solid-state (total) intermetallic compound layer development between 63Sn-37Pb solder and 100Au substrates. The value of y_0 was 0.3×10^{-6} m. The kinetic parameters were: $A = 1.156 \times 10^{-4}$ m-s ^{-0.54} ; $n = 0.54$; and $\Delta H = 31$ kJ/mol.....	88
1.79	Optical micrographs of the development of the intermetallic compound layer between 100Sn and Cu after aging for 200 days at temperatures of: (a) 70°C (158°F), (b) 100°C (212°F), (c) 135°C (275°F), and (d) 170°C (338°F). (e) Electron microprobe scan of the interface intermetallic compound layer chemistry from the Cu substrate to the solder field in the sample aged at 170°C (338°F) for 40 days. The traces of the Cu and Sn concentrations are shown in the plot	89
1.80	Optical micrographs of the intermetallic compound layers developed in solder/Cu diffusion couples that were aged for 400 days at 170°C (338°F): (a) 100Sn. (b) 63Sn-37Pb. (c) 95Sn-5Sb. (d) 96.5Sn-3.5Ag.....	90
1.81	Optical micrographs and electron microprobe traces of the intermetallic compound layer microstructure that forms between 58Bi-42Sn solder and Cu as a result of solid-state aging: (a) Micrograph, 85°C (185°F), 100 days. (b) Microprobe traces, 85°C (185°F), 100 days. (c) Micrograph, 120°C (248°F), 400 days. (d) Microprobe traces, 120°C (248°F), 400 days	93
1.82	Optical micrograph of the intermetallic compound that formed between 100In and Cu after solid-state aging at 100°C (212°F) for 350 days.....	95
1.83	(a) Optical micrograph of the intermetallic compound layer that formed between 50In-50Sn and Cu after aging for 200 days at 85°C (185°F). (b) Electron microprobe trace of Cu, Sn, and In elements at the interface between the Cu substrate and 50In-50Sn solder following aging at 100°C (212°F) for 200 days.....	95
1.84	Plots of the natural logarithm of the rate constant, k , as a function of the reciprocal temperature ($1/T$ in °K) for selected substrate alloys and solders: (a) 95Sn-5Sb. (b) 95Sn-5Ag. (c) 60Sn-40Pb. (d) 10Sn-90Pb (tabular format).....	97
1.85	Electron microprobe traces and SEM micrographs for hot solder dipped 63Sn-37Pb/Au couples that were solid-state aged for 90 days at: (a) 55°C (131°F). (b) 70°C (158°F). (c) 100°C (212°F)	99
1.86	Schematic diagram of the intermetallic compound layer morphology that develops by solid-state aging in the Au/50In-50Pb system.....	100
1.87	Plot of intermetallic compound layer thickness as a function of the square root of time for several metal substrates having an electroplated 100Sn layer. The aging temperature was 170°C (338°F).....	101
1.88	(a) Low- and (b) high-magnification scanning electron micrographs of the intermetallic compound layer formation between 60Sn-40Pb solder and Kovar™. The sample was aged at 170°C for 50 days. The interface reaction was comprised of the intermetallic compound formation: (#1) compound containing Sn, Fe, Ni, and Co and (#2 and #3) compound containing primarily Ni and Sn as Ni ₃ Sn ₄	102
1.89	Graphical representation of the intermetallic compound layer thickness of Sn-rich solders on Cu versus the Sn content of the solder for a homologous temperature of 0.88 and aging time of 400 days	102
1.90	Total intermetallic compound layer thickness as a function of solder Sn content for homologous temperatures of 0.25, 0.50, 0.75, and 0.90 and aging times of: (a) 50 days. (b) 100 days. (c) 200 days. (d) 400 days. The intermetallic compound layer thickness values were computed from the respective forms of Equation 1-29 as determined per the experimental data of each solder alloy	103
1.91	Peel strength of Cu and brass alloy solder joints made with 63Sn-37Pb alloy as a function of intermetallic compound (“reaction”) layer thickness. The soldering temperatures used to form the layer thicknesses were 265°C (510°F), 360°C (680°F), and 454°C (850°F).....	106
1.92	Schematic diagrams of several fundamental solder joint configurations.....	109
1.93	Plot of meniscus (capillary) rise as a function of the gap width between two Cu plates. A rosin- based flux was used in the tests. The solder alloys were: (1) “SnSb,” 95Sn-5Sb; (2) “SnPb” 60Sn-40Pb; (3) “SnAg,” 96.5Sn-3.5Ag; (4) “SnAgBi,” 91.84Sn-3.33Ag-4.83Bi; and (5) “SnCuAg,” 95.5Sn-4.5Cu-0.5Ag. X-ray radiographs were used to image the capillary rise by the solder	110
1.94	Plot of void content (as percentage of the joint’s projected area) as a function of the gap width between two Cu plates. A rosin-based flux was used in the tests. The solder alloys were: (1) “SnSb,” 95Sn-5Sb; (2) “SnPb” 60Sn-40Pb; (3) “SnAg,” 96.5Sn-3.5Ag; (4) “SnAgBi,” 91.84Sn-3.33Ag-4.83Bi; and (5) “SnCuAg,” 95.5Sn-4.5Cu-0.5Ag. X-ray radiographs were used to image the voids.....	110
1.95	Schematic diagram of the flow of liquid solder through a joint having a bend	111

1.96	Schematic diagram of cylindrical sleeve joints between dissimilar materials. The effect of thermal expansion mismatch between the two parts on the width of the gap during heating to the soldering temperature is illustrated for the two cases: (a) $\alpha_{\text{sleeve}} \gg \alpha_{\text{cylinder}}$ in which the gap widens. (b) $\alpha_{\text{sleeve}} \ll \alpha_{\text{cylinder}}$ in which the gap becomes smaller	112
1.97	Schematic diagram of the effect of molten solder surface tension on the alignment of: (a) One block atop another block with a solder film between them. (b) The centering of a cylinder and sleeve by solder in a lap joint.....	114
1.98	Schematic diagrams of self-jigging techniques in solder joint design.....	115
1.99	Schematic diagram of the behavior of molten solder at a substrate corner: (a) Solder has difficulty wetting around a corner and will often collect at the edge. (b) Deposited, solid solder films (e.g., electroplated coatings) will dewet from corners upon melting.....	116
1.100	(a) Schematic representation of thermal conduction (Q) from the hot surface (T_H) to the cold surface (T_C) of a solid cylinder having a cross section A and length l. (b) Illustration of thermal conduction and thermal convection causing heat loss from a lap joint	117
1.101	Heating case study for the soldering of two Cu rods together.....	118
1.102	Schematic diagram of (a) tension, (b) compression, and (c) shear loading configurations on a material. The original dimensions (solid lines); dimensional change, Δl , due to the imposed stresses; and the final dimensions (dashed lines) are also identified	121
1.103	Stress-strain curves.....	121
1.104	Schematic diagram of the three fundamental fracture mode loading regimes: (a) Mode I, tension. (b) Mode II, shear. (c) Mode III, “trouser-leg tear”	122
1.105	Creep deformation curves for stress σ_1 , $\sigma_2 > \sigma_1$, and $\sigma_3 > \sigma_2$. Each of the three creep regimes—primary (I), secondary (II), and tertiary (III)—are illustrated on the σ_1 curve	123
1.106	Schematic diagram of a butt joint undergoing a tensile load. (a) As the substrates pull apart, the natural tendency is for the solder to neck down. However, the extent of necking is constrained by the substrate, causing the solder to appear stronger (and less ductile) than it is as a bulk material. (b)The joint strength is dependent upon all structures in the joint, including the intermetallic compound layers and the interfaces that accompany each of the multiple layers	124
1.107	Plot of apparent tensile strength of butt joints that were made between Cu and 96.5Sn-3.5Ag solder, and were tested at 3.5 mm/min (0.14 in./min).....	124
1.108	Plot of apparent shear strength from ring-and-plug joints that were made between Cu and 96.5Sn-3.5Ag solder, and were tested at 3.5 mm/min (0.14 in./min)	125
1.109	Sinusoidal load history illustrating fatigue: (a) The generalized case. (b) The special case in which $\sigma_m = 0$	126
1.110	S-N fatigue curves for a mild steel and an Al alloy. Note that the steel has a well-defined <i>fatigue limit</i> while the Al alloy appears to gradually approach a stress level limit.....	127
1.111	Fatigue data for bulk 63Sn-37Pb, plotted as cycles to failures versus plastic strain range.....	128
1.112	Schematic diagram of the representation of tensile/compressive and shear residual stresses in the solder joints due to thermal expansion mismatch between the two members. The case of heating is illustrated and $\alpha_1 > \alpha_2$: (a) A lap joint. (b) A cylindrical solder joint.....	129
1.113	Fatigue life curve from data of 60Sn-40Pb solder that was tested at -50°C (-58°F), 35°C (95°F), and 125°C (257°F). $\Delta\gamma_p$ is the plastic strain range; N_f is the number of cycles to failure (failure = 50% load drop).....	130
1.114	Frequency-dependent fatigue life of 60Sn-40Pb solder at 35°C where ν is the frequency and N_f is the number of cycles to failure (failure = 50% load drop)	132
1.115	Photograph of corrosion activity on a solder joint made between 96.5Sn-3.5Ag solder and Cu base materials caused by flux residues.....	132
1.116	Galvanic series for several metals and alloys in seawater.....	136
1.117	Schematic diagram of the idealized galvanic corrosion cell.....	137
1.118	Schematic diagram of a solder joint with a potential to cause galvanic corrosion. The tube-joint structure (a) is broken down into the metal couples between the solder and the substrate materials (b) that are covered with the electrolyte.....	140
1.119	(a) Two metals of the same composition are immersed into an electrolyte. Both exhibit similar corrosion behaviors (e.g., mechanisms, rates, etc.). (b) When a voltage is applied between the two metal members, the strip connected to the positive terminal will provide the oxidation half reaction and corrode.....	141

1.120	The process of electromigration between two metals under an applied electrical potential.....	141
1.121	Schematic diagram of corrosion process caused by a breach in the protective finish	143
1.122	Density of molten solder alloys as a function of solder temperature. The solid density is taken as that value found at the melting point of the alloys	145
1.123	Schematic diagram of the thermogram provided by the differential scanning calorimeter (DSC). Vertical deviations above zero are endothermic (energy input) reactions; deviations below the zero point are exothermic reactions (energy release).....	148
1.124	Schematic diagrams of observed peak configurations in the DSC are shown in (a), (b), and (c). (d) Schematic diagram of DSC curves anticipated by the various compositions on the hypothetical, simple eutectic binary alloy phase diagram: eutectic (A-A') and noneutectic (B-B' and C-C") melting events	150
1.125	Plot of surface tension as a function of temperature for molten 100Sn and several liquid Sn-Pb alloy compositions.....	152
1.126	Plot of solder-flux interfacial tension as a function of Sn content in Sn-Pb solders for an organic (rosin) flux and an inorganic acid (ZnCl ₂ -based) flux. The solder temperature was 400°C/752°F. The two measurement techniques were the sessile drop (SD) and the maximum bubble pressure (MBP) procedures	153
1.127	Schematic diagram of the maximum bubble pressure (MBP) test for surface tension. In this case, the interfacial tension between the fluid #1 (flux) bubble and the fluid #2 (molten solder) would be measured.....	153
1.128	Techniques to evaluate the viscosity of a fluid: (a) Rotating cylinders. (b) Rotating disks. (c) Tube-type (Saybolt). (d) Falling-sphere	156
1.129	Optical micrographs of the three cases of solder wetting: (a) Excellent wetting. (b) Dewetting. (c) Nonwetting	158
1.130	Schematic diagram of the area-of-spread solderability test	159
1.131	Solderability test for conductive features on printed circuit boards, using solder flow down a metal strip	159
1.132	Parallel plate, capillary rise solderability test: (a) Schematic diagram of sample construction and testing. (b) An X-ray micrograph of the test sample, showing the extent of capillary rise (h) and the void content in the gap	160
1.133	(a) Capillary rise as a function of gap width for the test sample shown in Figure 1.132a. The solder compositions were: 95Sn-5Sb (SnSb), 63Sn-37Pb (SnPb), 96.5Sn-3.5Ag (SnAg), 91.84Sn-3.33Ag-4.83Bi (SnAgBi), and 95.5Sn-0.5Ag-4.0Cu (SnAgCu). (b) The percent of the projected area of the gap that has voids	161
1.134	Schematic diagram of the rotary dip test to evaluate the solderability of holes in through-hole printed circuit boards	162
1.135	Schematic diagram of the globule solderability test method for wires.....	162
1.136	Schematic diagram of a wetting balance system. A stepper motor raises the solder pot to initiate the test, and then lowers it upon completion of the test	163
1.137	Schematic representation of the molten solder meniscus that rises on a plate (coupon) sample geometry that was immersed edge-on into the molten solder bath as part of the wetting balance test	164
1.138	Wetting balance curve of meniscus weight as a function of time. The various points along the curve (A, B, and C) pertain to the position of the solder meniscus as shown in the insert diagrams	164
1.139	Schematic diagram of the meniscometer technique used to measure the meniscus height, H, on a sample immersed into a bath of solder.....	164
1.140	Schematic diagrams of popular shear and tensile test configurations used to evaluate the respective strengths of solder joints	168
1.141	Four-point bend test sample "B" geometry and test configuration per MIL-STD-1942A	169
1.142	Torsion test configuration for: (a) A sleeve joint. (b) A butt joint	170
1.143	Schematic diagram of the T-peel test sample and data output	171
1.144	"Dupont" pull test for measuring the strength of thin and thick film finishes: (a) Schematic diagram. (b) Photograph of the test specimen.....	171
1.145	(a) Schematic diagram of the compact tension (CT) test sample configuration. (b) Logistics for data analysis of the fatigue crack growth	172

1.146	Schematic diagram of the CT test specimen for solder joint testing	173
1.147	Test geometries using dissimilar substrate materials to impose thermal fatigue in solder joints under temperature cycling environments: (a) Shear, (b) Tension, and (c) Mixed mode	173
1.148	Schematic diagrams of the Charpy and IZOD impact test configurations, the samples of which were modified with a solder joint.....	174
1.149	Schematic diagrams for: (a) Single-edge notch bar (SENB). (b) The compact tension (CT) specimen geometry for fracture toughness testing.....	175
1.150	Fracture morphologies of solders: (a) Microvoid coalescence via large scale plasticity in the tension test of 63Sn-37Pb solder. (b) Moderate plasticity observed in the tensile failure of 72.9Pb-15.2In-11.9Sn solder. (c) Transgranular fracture with limited ductility from a tensile test of the 96.5Sn-3.5Ag solder. (d) Shear failure of a 63Sn-37Pb solder joint. (e) Interfacial failures at the Ni/63Sn-37Pb solder interface and a failure between the solderable finish (Ni) and the underlying base material (thick film Ag-based frit)	177
1.151	T-peel fracture surface of a Cu sample made with 60Sn-40Pb solder. The surface shows the intermetallic compound layer grain pattern resulting from the fracture path cutting through it	178
1.152	Optical micrographs of phase boundary and grain boundary sliding arising from (thermal) fatigue of: (a) 58Bi-42Sn solder. (b) 91.84Sn-3.33Ag-4.83Bi alloy	178
2.1	Schematic diagram showing the relationship between service temperatures, processing temperatures, and the melting properties of the solder	180
2.2	Schematic diagram illustrating the relationship between the total electrical resistance and geometry of the serial structure of Cu, solder, and Al	181
2.3	Optical micrographs showing the precipitated Cu ₆ Sn ₅ particles in a 95.5Sn-4.0Cu-0.5Ag solder	183
2.4	SEM micrograph of AuSn ₄ needles resulting from the solid-state precipitation reaction between Sn and Au	183
2.5	SEM micrograph of intermetallic compound particles formed between Sn and Sb	184
2.6	Contact angle of molten Sn on Cu as a function of reaction time and temperature.....	191
2.7	Tensile strength and ductility for 100Sn, 60Sn-40Pb, and 10Sn-90Pb alloys as a function of test temperature.....	199
2.8	(a) Tensile strength, yield strength, ductility and (b) tensile modulus and Poisson's ratio of 63Sn-37Pb solder as a function of temperature	203
2.9	Isothermal fatigue life (N _f) of bulk 60Sn-40Pb solder, as a function of plastic strain range	204
2.10	Room-temperature fatigue life of bulk 60Sn-40Pb solder, as a function of applied stress.....	204
2.11	(a) Lap shear strength (0.2 mm gap, rate unknown) and (b) Vickers hardness (100 g load) data for 63Sn-37Pb/Cu joints and 63Sn-37Pb bulk solder, respectively, aged at room temperature	208
2.12	Tensile strength of Sn-Pb-Sb alloys as a function of room-temperature aging.....	210
2.13	Hardness of cast 47Sn-47Pb-6Sb alloy after room-temperature aging.....	210
2.14	Bulk tensile strength and elongation of 95Sn-5Sb as a function of the test temperature	213
2.15	Bulk creep rupture test data for 96.5Sn-3.5Ag solder.....	215
2.16	Copper ring-and-plug creep rupture test data for 96.5Sn-3.5Ag solder.....	215
2.17	Room-temperature shear strength of Zn-0.74Cu and 60Sn-40Pb solders as a function of displacement rate.....	217
2.18	Binary alloy phase diagrams for: (a) The Au-Ge and (b) Au-Si systems	225
2.19	Temperature-dependent: (a) Bulk yield strength. (b) Bulk ultimate tensile strength. (c) Ductility of Au-Sn, Au-Si, and Au-Ge eutectic solders. The test rate was 0.5 mm/min (0.02 in./min)	227
3.1	Schematic diagram of the processes occurring at the front of spreading molten solder on a substrate having a protective metal finish. The process is comprised of the sequence of: (a) Wetting and spreading by the molten solder over the protective finish. (b) Dissolution of the protective finish into the molten solder. (c) Wetting by the molten solder to the base material surface	230
3.2	Schematic diagram of the processes occurring at the front of the spreading molten solder on a coated base material. The molten solder takes part in the following sequence of processes: (a) Wetting the protective finish. (b) Dissolution of the protective finishes. (c) Wetting of the solderable coating. (d) Some dissolution of the solderable coating as a normal part of wetting	235

3.3	Schematic diagram of the layer stacking for soldering to a ceramic, nonwetttable surface. The adhesion layer serves to attach the solderable (plus protective) metal coatings to the nonmetallic substrate material	236
3.4	Schematic diagram of the thick film layer that provides the solderable surface for the soldering of ceramic substrate. The adhesion layer has been exaggerated in relative thickness; in most cases, it is not visible in the optical microscope	237
3.5	Kinetics plots and equations for solid-state intermetallic compound layer growth for: (a) 100Au/63Sn-37Pb solder. (b) 76Au-21Pt-3Pd/63Sn-37Pb couples. The Au and Au-Pt-Pd base materials were used in sheet form.....	239
3.6	Precipitation hardening graphs of (a) ultimate tensile strength and (b) hardness vs. aging time and temperature for the 97.7Cu-1.9Be-0.4Ni alloy	246
3.7	Through-hole solder joints made by Cu foil/electroless Cu/electroplated Cu construction as shown in: (a) A low magnification view of the joint geometry. (b) A high magnification view of the layer structure (neighboring joint). Built-up electroless Cu/electroplated Cu technology as shown in: (c) A low magnification view of the joint geometry. (d) A high magnification view of the layer structure (neighboring joint)	247
3.8	(a) SEM and (b) optical micrograph cross section of the solder joint of a small outline integrated circuit (SOIC) package showing the Cu leads	248
3.9	Flow chart for the precleaning of stainless steels.....	259
3.10	Precipitation hardening aging curves of <i>tensile strength</i> for: (a) 2024 and (b) 6061 wrought Al alloys.....	267
3.11	Schematic diagram of the abrasive soldering procedure.....	271
3.12	Schematic diagram of the set-up for ultrasonic soldering: (a) Horns immersed into the solder pot, including pertinent geometric parameters. (b) An ultrasonic soldering “pot.”	272
3.13	Solder rise in a gap by ultrasonic activation is limited in height to equality with the level of the solder bath. Buoyancy provides the driving force.....	273
3.14	(a) Schematic diagram illustrating corrosion of an Al alloy base metal having a Cu or Ni solderable finish only. (b) Improved corrosion resistance of Al alloy having the Cu or Ni solderable finish plus a Cd or Zn anodic layer.....	274
3.15	Effect of exposure to high temperatures and prolonged time periods on the: (a) tensile strength and (b) yield strength of AZ31B-H24 Mg alloy	278
3.16	Optical micrograph of the microstructure of a 50-50 Al ₂ O ₃ /Mo cermet. The light phase is the Al ₂ O ₃ ; the dark phase is the Mo component.....	287
3.17	Schematic diagram of the firing process of a thick film ink, showing the segregation process whereby most of the glass adhesion material diffuses to the ink/ceramic substrate interface. The metal component forms the solderable coating	289
3.18	Plot of solid-state, intermetallic compound layer growth rates as a function of temperature for the Au/50In-50Pb and Au-3Pd/50In-50Pb systems. The growth kinetics are linear with time in both cases	290
4.1	Schematic diagram of a tube-and-sleeve joint that illustrates the application of flux and the flow of solder during a hand soldering process	294
4.2	Schematic diagram of a tube/manifold joint that has been soldered from both sides. The first joint (a) solidifies and forms a blockage that prevents flux and volatiles from escaping the joint	296
4.3	Schematic diagram illustrating the process of a reactive flux; Al is exemplified in this case	304
4.4	Schematic diagram of the application of an inert gas blanket to exclude the air atmosphere from the immediate vicinity of a solder joint.....	306
4.5a	Vapor pressure/temperature chart for several elemental metals.....	307
4.5b	Vapor pressure/temperature chart for several elemental metals.....	308
4.5c	Vapor pressure/temperature chart for several elemental metals.....	309
5.1	Schematic diagram of the application methods for solder paste: stencil or screen printing and dispensing.....	311
6.1	Schematic diagram showing the preference for solder flow <i>parallel</i> to grooves and the limited flow perpendicular to them: (a) Sessile drop on a flat plate. (b) Scratches parallel to the tube axis that accentuates of solder flow vs. (c) circumferential scratches or grooves perpendicular to the tube axis that will hinder solder spreading.....	317

6.2	Schematic diagram of the logistics for identifying a suitable solder and developing a soldering process to make the joint.....	321
6.3	Schematic diagram of the (a) recommended and (b) not recommended clamp position when cutting or forming a workpiece having a solder joint in it.....	323
6.4	Schematic diagram of two types of soldering iron: (a) Electrical resistance heat source. (b) Flame source.....	324
6.5	Schematic diagram of a water tank that illustrates the input reservoir and drain of thermal energy in a soldering iron situation.....	325
6.6	Schematic diagram depicting the soldering of two Cu rods to illustrate the computation of soldering iron power rating vs. joint configuration and desired temperature rise.....	328
6.7	Four basic geometries of soldering iron tips: (a) Chisel. (b) Conical. (c) Pyramid. (d) Ball.....	329
6.8	Schematic diagram of the contact geometry between the soldering iron tip and flat or round surfaces.....	329
6.9	Schematic diagram of the manual soldering of a pin/collar assembly, using a soldering iron.....	330
6.10	Schematic diagram of techniques to control the concentricity between a tube and a collar: (a) spacer wires and (b) fixturing.....	332
6.11	Schematic diagram showing preferred orientation of the workpiece to assist solder flow by the action of gravity.....	333
6.12	Through-hole circuit board for telecommunications applications.....	333
6.13	Schematic diagrams of some of the leaded component package configurations used in through-hole electronic circuit boards.....	334
6.14	Schematic diagram of single-sided, double-sided and multilayer through-hole solder joints found on electronic circuit boards.....	334
6.15	Schematic diagram of the through-hole solder joint, including material and structural details.....	335
6.16	Photographs of four conditions of a fuel gas of flame: (a) Pure gas (acetylene) flame burning solely on O ₂ from the air. (b) Carburizing flame. (c) Neutral flame. (d) Oxidizing flame.....	337
6.17	Photographs of the torch soldering process for a tube-and-fitting: (a) Determining the proper tube lengths. (b) Removing burrs and flash from the cut surfaces. (c) Cleaning (sanding) the tube section (exterior surface). (d) Cleaning the fitting section with a brush (interior surfaces). (e) Applying flux to the tube section (exterior surface). (f) Applying flux to the fitting section (interior surface). (g) Assembling the tube and fitting. (h) Heating the assembly. (i) Performing the soldering operation.....	338
6.18	Schematic diagram of the effects of tube distortion on the solder joint: (a) Concentric parts. (b) Regions of poor fit-up (minimum gap) and overly large gaps will prevent the formation of a satisfactory solder joint when distorted tubes are used.....	339
6.19	Schematic diagram of the process by which a solder joint of horizontal orientation is made: (a) Solder is reflowed at the bottom of the joint which solidifies to establish a “dam.” (b) Form the joint from the “8 o’clock” position to the “12 o’clock” position. (c) Complete the joint by soldering from the “4 o’clock” position to the “12 o’clock” position.....	341
6.20	Schematic diagram of soldering joints of cylindrical geometry so as to avoid residual stress buildup: (a) Tube and sleeve assembly. (b) Solder one half of the circumferential gap in a counterclockwise direction. (c) Complete the other half of the gap, starting at the same place and moving in a clockwise direction.....	341
6.21	Schematic diagrams of typical joint geometries that are frequently assembled by torch soldering (keep in mind that orientations of the joint gap can be vertical or horizontal): (a) Cylindrical butt joints. (b) Plate butt joints. (c) Lap joint (which includes the tube-and-sleeve joint or other cylindrical geometries).....	343
6.22	Schematic diagram illustrating the preplacement of solder preforms at the entrance of the joint gap that will allow the solder to fill by capillary action, thus ensuring the removal of flux volatiles. The chamfer on the part eliminates the corner edge, thus facilitating solder entry into the gap.....	345
6.23	Schematic diagram of the surface tension effect by molten solder for aligning parts during formation of the joints. (Additional illustrations are found in Figure 1.97.).....	349

6.24	Schematic diagram of the steps in an automated, torch soldering process: (a) Fluxing followed by (b) assembly of the parts. (c) Torch soldering process. (d) The finished solder joint.....	350
6.25	Schematic diagrams of the batch furnace (a) and in-line furnace concepts (b, c). The in-line furnace can use radiation/convection heat modes (b) or thermal conduction (c).....	351
6.26	Schematic diagram of an idealized furnace process (solid plot) and the more likely profile (dashed plot)	355
6.27	Ellingham diagram.....	358
6.28	Schematic diagram illustrating the use of a weight to “mechanically” assist the wetting and spreading of the solder	360
6.29	Schematic diagram of the preheat stage of a soldering process: (a) A single, continuous heat up to a preheat temperature hold. (b) Preheat stage comprised of a series of smaller ramp/hold combinations.....	364
6.30	Schematic diagram of a temperature cycle showing “overshoot,” “undershoot,” and “ringing” at the conclusion of a temperature ramp.....	364
6.31	SEM optical micrograph of an electronic solder joint illustrating the formation of solder balls	365
6.32	Modification to the preheat step to accommodate the higher temperature solders. The steady ramp may also be replaced with a sequence of ramp/hold segments (see Figure 6.29)	367
6.33	Schematic diagrams of distortion resulting from differential heating rates and part geometry: (a) Parts of varying sections with the thinner section heated up more rapidly than the thicker section. (b) Outer surface is heated more rapidly than the interior of a thick section. (c) Nonuniform heating through the material (top-to-bottom) results in a warping of the part. In each case, the outer areas that were more rapidly heated will be distorted by compressive stresses generated at T_1 and residual tensile stresses at T_0	373
6.34	Schematic diagram illustrating the use of the interlayer in a dissimilar metal solder joint as a means of reducing the residual stress levels. The thermal expansion coefficient of base material #1 (α_1) is less than that of base material #2 (α_2). $\Delta T < 0$ indicates conditions for a cooling step. Deformation by the interlayer material reduces the magnitude of the thermal expansion mismatch residual stresses between base materials #1 (compressive) and #2 (tensile).....	377
6.35	Schematic diagrams of approaches to fixturing solder joints: (a) Wiring the two substrates together with a preform. The gap dimension can be maintained by a spacer of wettable wire placed in the gap (b). Shown in (c) and (d) are more elaborate fixturing for controlling the joint.....	378
6.36	Assortment of configurations for self-jigging the substrates used in a solder joint.....	380
6.37	Schematic diagram of techniques to reduce friction forces between the workpieces and the fixturing: (a) Vertical orientation replaces the horizontal arrangement. (b) Rollers to reduce friction	383
6.38	Schematic diagram of a retort. The retort design must be able to withstand vacuum and positive pressure internal environments when used	384
6.39	Schematic diagram of the condensation of water vapor into liquid as a function of decreasing temperature. The condensation (phase change process), which starts at point B with 100% vapor and is completed at point C with 100% liquid, takes place entirely at the same temperature, 100°C (212°F).....	385
6.40	Schematic diagram of the vapor phase reflow apparatus. Only a single fluid is present in this illustration	386
6.41	Schematic diagram of the use of photoresist films for the selective deposition of solder coatings by the dipping process.....	390
6.42	Schematic diagram of: (a) the “not recommended” technique and (b) the “preferred” technique to dip solder parts having a <i>blind</i> hole or gap. In case (b), the angle θ should be sufficiently large to allow solder to gradually fill the hole before the opening is covered by the bath.....	391
6.43	Schematic diagram of the solder breakaway as a part is withdrawn from the molten solder bath: icicle formation (a-c) and bridge formation (d-f).....	392
6.44	Schematic diagram of two orientations of a part being withdrawn from the solder bath: (a) 0° angle that has the propensity to form icicles and bridges and is not recommended. (b) Withdrawal at an angle $>0^\circ$ allows a “peel back region” that minimizes icicle and bridge defects	394

6.45	Schematic diagram of the penetration radius of the molten solder in a concave corner for a part immersed into the molten solder bath. The immersion depth is Δh and the solder surface curvature, R	395
6.46	Schematic diagram of the drag soldering process.....	397
6.47	Schematic diagram of the wave soldering apparatus	398
6.48	Schematic diagram of the solder wave as exemplified by an electronic part. The three positions in the wave, the entry region (A), the soldering region (B), and the “peel-back” region (C) have well-defined properties that are all important toward minimizing solder joint defects.....	399
6.49	Schematic diagram of the more widely used solder wave geometries: T-wave, extended T-wave; lambda wave; and the dual wave	400
6.50	Schematic diagram showing part directions with respect to the solder wave for making a “proposed solder joint.” (a) The preferred direction is “B.” (b) Using direction “A” will result in the possibility of the wettable area being skipped by the solder wave	401
6.51	Schematic diagram of the hot air level process to produce thin solder coatings on workpieces. This procedure has also been developed with the horizontal orientation as an in-line process.....	402
6.52	Schematic diagram of a sample and coils for induction soldering	406
6.53	(a) Schematic diagram of the magnetic field created along a section of electrical conductor attached to a DC voltage (battery). Note the relationship between the direction of the current in the conductor and the direction of the magnetic field lines. (b) Steady magnetic field resulting from current passing through a coil conductor	408
6.54	Schematic diagram of the formation of eddy currents in a conductive piece of material (e.g., iron) when it is placed into the <i>alternating</i> magnetic field	409
6.55	Schematic diagram showing the formation of eddy currents set up by the induction coil and are located along the surface of the material (“skin effect”).....	410
6.56	Schematic diagrams illustrating the effects of (a) coil proximity, x and (b) coil pitch, N/L , on the heated zone in the workpiece	411
6.57	Schematic diagrams of various coil geometries and workpiece configurations	412
6.58	Schematic diagram of the use of coil/workpiece separation (x) and coil pitch (N/L) to adjust the initial heat (temperature) distribution in the workpiece. Sample conditions include: (a) Uniform separation (x) and uniform pitch (N/L). (b) Nonuniform x , uniform N/L . (c) Uniform x , nonuniform N/L . (d) Edges and corners that become regions of flux line concentrations and have the potential to be “hot spots” there.....	413
6.59	Schematic diagram of the use of shielding to remove the magnetic field influence from the workpiece	414
6.60	Schematic diagram of the effects of an electric field E on the charge distribution (dipoles) that polarize (P) a material as the basis for microwave heating.....	417
6.61	Schematic diagram of the resistance heating process for the lap joint geometry. A higher magnification view of the joint region shows the surface asperities typically present on the substrate and solder where they form the mutual interface(s)	418
6.62	Schematic diagram of resistance heating of a bi-material joint in which one of the materials is not electrically conductive. The electrodes are used to heat the electrically conductive substrate material. The nonconductive material is “proximity” heated by conduction from the first substrate material	421
6.63	The electromagnetic spectrum; frequency is represented on the left vertical axis and the corresponding wavelength is represented on the right vertical axis.....	424
6.64	Percent reflectance (or transmittance) as a function of light wavelength for a number of materials.....	425
6.65	(a) Photograph of an ultrasonic soldering apparatus with a (Cu) substrate in place above the solder bath, centered between the horns. (b) Schematic diagram of the system in (a)	429
6.66	(a) Schematic diagram illustrating the limited meniscus rise on a vertical surface under ultrasonic activation and in the absence of a flux. (b) The sample is immersed into the bath. The buoyancy force causes some intimate contact between the molten solder and the bottom edge of the coupon so that ultrasonic action can remove the oxide layer. (c) The buoyancy force drives the meniscus rise to the same level as the bath, but no further as the buoyancy force is lost.....	430

6.67	Capillary rise as a function of gap width for Cu samples exposed to 60Sn-40Pb solder (250°C/482°F) for 15 s of ultrasonic activation. The baseline samples used a rosin-based, mildly activated flux coating on the substrate surface prior to immersion in the bath. No ultrasonic activation was used in this latter case.....	431
6.68	Schematic illustration depicting the cleaning action of saponifier (detergent) molecules. The saponifier molecule attaches to the residue by an organic bond. The slightly polar nature of the saponifier molecules causes them to also be attracted to the water molecules. The water molecule removes the saponifier molecule along with the residue particles from the surface.....	439
6.69	Cascade washing process. The part moves “uphill” to successively cleaner baths until it is fully cleaned at the end of the process line	440
7.1	Optical photographs of electronic (through-hole) solder joints made of: (a) 63Sn-37Pb solder. (b) 96.5Sn-3.5Ag solders. The fillet of the latter solder joints have a duller surface appearance, owing solely to the composition	448
7.2	Schematic diagram illustrating poor solder wetting/spreading (solderability). (a) This defect is represented by poor fillet rise on vertical surfaces and inadequate spreading over the solderable surface (i.e., the surface that was intended to be covered). (b) Poor solderability may also appear as an incomplete filling of gaps or holes.....	449
7.3	Schematic diagram showing void formation in a solder joint. Voids that intersect the fillet surface are referred to as “blowholes.” Sidebar (b) illustrates the formation of a void caused by volatile and/or gas formation. A thin solder film forms at the substrate surface. However, when such voids are formed by nonwetting conditions, the solder film is absent from the culprit surface	450
7.4	Schematic diagram of bleed or inspection holes in a substrate that are used to monitor the progress of solder flow down a long gap or hole	456
7.5	SEM micrograph of a Cu strap soldered to the anode end of a PIN diode	457
7.6	(a) Optical micrograph of the microstructure of a Sn-Ag-Bi solder, showing the Ag ₃ Sn particles in the Sn-rich matrix. (b) SEM micrograph of a similar region on the alloy, still showing the Ag ₃ Sn particles but also, clearly delineating the white Bi-rich zones in the matrix which are not visible in (a)	458
7.7	Schematic diagram of the equipment configuration for X-ray radiography. X-rays are generated at the X-ray tube source. They pass through a collimator so as to give them a consistent direction of propagation. The X-rays pass through the workpiece; the exiting X-rays are then captured on photographic film.....	459
7.8	Schematic diagram detailing the passage of the X-rays through the workpiece. Where there is more workpiece mass, there is a greater extent of scattering of the X-rays away from their initial “line-of-sight,” and therefore, a lower intensity of X-rays exiting the part to strike the photographic plate behind it.....	460
7.9	A “reverse-positive” print, that is, the image as it would be seen in the actual X-ray film (which is the negative) of a 75 μm (0.003 in.) thick solder joint that was formed between two Cu plates, each being 0.51 mm (0.020 in.) thick. The extent of flow by solder (60Sn-40Pb) is delineated by the brighter area. The dark circles in the joint are voids. The spacer bars (3) used to set the gap are visible at the top of the photograph.....	461
7.10	Schematic diagram of ultrasonic inspection. The system typically rests in a fluid to facilitate the transmission of waves to and from the workpiece. Incident sonic waves from the source as it scans the part, strike the workpiece and are transmitted through it. Discontinuities in the part structure (e.g., a void in the solder joint) disrupt that transmission, resulting in the reflection of some energy back to the source. The detector which scans at the opposite side of the part (transmission mode) detects the region of depleted sonic energy as a potential defect	462
7.11	Schematic diagram illustrating the scattering process responsible for ultrasonic imaging. The scattering of incident sonic energy occurs at the interfaces of mass changes in the structure. Although the scattering process at the base material/void interface has been highlighted, a similar process (of different magnitude) will also occur at other interfaces such as at the base material/solder interface	463

7.12	(a) Photograph of a workpiece comprised of two ceramic plates (one is underneath) soldered to a stainless plate. (b) Transmission mode ultrasonic image of the assembly. Low attenuation, that is, low signal loss, (light gray to white) indicates a good bond while high attenuation (dark gray to black) illustrates the poor bond areas. (c) X-ray radiograph of the same part, illustrating that the X-ray technique is ineffective at discerning bond defects in the joints	464
7.13	Schematic diagram of the reflecting (pulse-echo) technique. The bond on the same side as the source/detector combination is analyzed. Specifically, any signal attenuation will occur from the ceramic/solder interface since it is the first discontinuity struck by the incident waves	465
7.14	Schematic diagram of the thermal (heat) conduction through a part having a solder joint. The presence of a void causes a local loss in heat conduction efficiency that appears as a “cool spot” by the detector on the side opposite to the source.....	466
7.15	Schematic diagram of the thermal transfer technique for inspection of a fin/tube solder joint. The measured values of T_{fin} , T_o , and, T_f are compared against theoretical computations or baseline experimental data to determine the integrity of the solder joint(s).....	467
7.16	Schematic diagram of the setup to assess butt joint integrity by thermal transfer technique. Theoretical computations or baseline data are compared to the measured values of T_o and T_f to determine the heat transfer efficiency of the solder joint	468
7.17	(a) Photograph of the <i>macrostructure</i> of a connector in cross section, showing the pins that were soldered into the housing. (b) Optical micrograph of the cross section of the <i>microstructure</i> of the solder joints	472
7.18	Schematic diagram showing the diametrical and longitudinal (axial) cuts of a tube/sleeve lap solder joint configuration	474
7.19	Schematic diagram showing the taper section technique.....	475
7.20	Schematic diagram showing preferential polishing (or “polishing relief”) followed by substrate rounding in a solder joint metallographic specimen.....	475
7.21	Schematic diagram of rounding of a solder film, and the use of a protection layer to prevent the preferential loss by the solder material.....	476
7.22	Schematic diagram of the process of particle pull-out arising from the polishing process of solder alloys and solder joints.....	477
7.23	Optical micrographs of 63Sn-37Pb/Cu solder joints in: (a) The as-polished condition. (b) The polished and etched condition. The etching procedure was 3 s in a solution of (60 mL ethanol, 30 mL deionized H ₂ O, 5 mL HCl, 2 gm FeCl ₃) followed by 5 s in a solution of 25 mL DI H ₂ O, 25 mL NH ₄ OH, 1 mL 30% H ₂ O ₂)	478
7.24	Schematic diagram of oblique illumination that is used in light microscopy. Bright field illumination occurs when $\theta = 0^\circ$	480
7.25	(a) Bright field image of the deformation features surrounding a Vicker’s microhardness indentation made into a polished, Sn-Ag-Bi solder sample. (b) The same indentation was viewed with differential interference contrast microscopy; the deformation is more clearly delineated by this technique	481
7.26	Transmission electron micrographs of 63Sn-37Pb solder after cooling at 100°C/min/180°F/min: (a) Lower magnification view showing the Pb-rich phase particles between which are dislocation columns that develop into low-angle grain boundaries in the Sn-rich matrix. (b) Higher magnification view of the dislocation column in the Sn-rich matrix, between two Pb-rich particles.....	482
7.27	Schematic diagram of a progressive cross section through a lap joint by successive grinding and polishing steps on a single specimen mount. Spacer wires placed a specific distances during the encapsulation of the part will allow for a determination of the distance into the joint that is reached per each polishing step.....	483
7.28	Schematic diagram of a longitudinal (axial) section through a tube-and-sleeve joint that is off-axis. Quantitative measurements of the interface microstructure may be inaccurate due to the offset.....	484
7.29	Optical micrograph of the solder/substrate interface between 100In solder and Cu substrate after aging at 100°C (212°F) for 10 days. Of interest is the presence of (dark) polishing particles that have become embedded in the 100In field.....	484

7.30	Schematic diagram of voids in a solder joint undergoing mechanical testing. The footprint area of the voids represent the amount of load-bearing area that is lost.....	486
7.31	Schematic diagram of the effect of a crack on solder joint strength.....	487
7.32	Schematic diagram of the mechanical test geometry of a butt joint. The mixed deformation modes of tensile and shear would preclude any fundamental interpretation of the strength value, such as a conversion of maximum loads into stress levels for comparison with other tabulated data	488
7.33	SEM micrograph of the fracture path that formed when the Cu lead above was peeled from the alumina substrate. The arrows indicate the loading direction applied to the part. The fracture path is observed to have started at the interface between the solder and the Au-Pt-Pd thick film conductor and propagated from left-to-right in the photograph.....	489
7.34	Schematic diagram of a workpiece section after desoldering. The layers include the retained solder film on top, the intermetallic compound layer and the base material at the bottom	494
7.35	Schematic diagram of voids, cracks, and delamination (“pull-away”) in a tube-sleeve joint.....	498
A.1	Schematic diagram of the specimen geometry used to illustrate the computation of thermal expansion residual stresses in the base material layers (1) and (3) and solder layer (2): (a) undeformed condition and (b) deformed condition in which expansion/contraction occurs linearly with position y . The parameters, a_i , represent the individual layer thicknesses.....	514
C.1	(a) 100 Sn (etched for grain boundary delineation); (b) 97Sn-3Cu	517
C.2	85Sn-15Pb.....	518
C.3	63Sn-37Pb.....	518
C.4	(a) 60Sn-40Pb; (b) 62.5Sn-36.1Pb-1.4Ag; (c) 62.5Sn-36.1Pb-1.4Ag (aged as part of a solder joint, cooling rate unspecified).....	519
C.5	(a) 95Pb-5Sn (unetched); (b) 95Pb-5Sn (etched).....	520
C.6	95Sn-5Sb.....	520
C.7	(a) 96.5Sn-3.5Ag; (b) 95.5Sn-0.5Ag-4.0Cu; (c) 91.84Sn-3.33Ag-4.83Bi	521
C.8	91Sn-9Zn.....	522
C.9	96Zn-4Al (representative of the 94Zn-6Al eutectic composition).....	522
C.10	(a) 50In-50Pb; (b) 90Pb-5In-5Ag.....	522
C.11	(a) 52In-48Sn (includes black polishing particles); (b) 70 Sn-18Pb-12In.....	523
C.12	(a) 58Bi-42Sn (10°C/min); (b) 58Bi-42Sn (aged as part of a solder joint, cooling rate unspecified)	523
C.13	66In-34Bi	524
C.14	43Sn-43Pb-14Bi.....	524
C.15	80Au-20Sn (lightly etched).....	524
C.16	88Au-12Ge.....	524
C.17	98Au-2Si (representing the 97Au-3Si eutectic composition)	525
C.18	95Cd-5Ag (DIC image)	525
C.19	68Sn-32Cd (DIC image)	525
C.20	44In-42Sn-14Cd.....	525
D.1	The thermocouple circuit	526
D.2	The multileg thermocouple circuit.....	526
D.3	Measurement of a part temperature using two junctions of the thermocouple that are formed across the part. The temperature measurement is accurate, so long as the entire part is at a uniform temperature, assuring that the two junctions are at the same temperature	527
D.4	Various techniques for securing a thermocouple junction to a workpiece.....	528

AWS Soldering Handbook

1. Fundamentals of Soldering Technology

1.1 Introduction

Joining processes, which attach two or more substrates or base materials together, be they metals, ceramics, or plastics, can be considered as coming under one of two generalized methodologies: *filler material joining*, or *fusion joining*.

Filler material joining refers to the use of a third material to form a bond between the two base materials, and includes the processes of *soldering*, *brazing*, and *adhesive bonding*. The filler material must adhere to both base materials in order to effect an adequate bond. Although the bonding mechanism in such cases may cause chemical changes at the substrate material surfaces in order to promote adhesion, *at no time does the temperature of the substrates exceed their respective melting points*.

When the melting temperature of the substrate material is exceeded, the bond is formed by a *fusion joining* process, e.g., welding. In welding, the two substrates are joined by the intermixing of their mutually molten segments. A third material, also referred to as a filler material, may be simultaneously melted and added to the molten base materials.

Because metals have been an integral part of engineered structures since the dawn of civilization, filler material joining processes have a long history of use with these base materials. However, filler metal joining methodologies have also been applied to the other materials subsets, including ceramics and plastics.

Soldering and brazing are high-temperature filler metal processes that are used in many engineering applications. The difference between soldering and brazing is defined by the melting temperature of the filler metal. A filler metal which has a liquidus temperature below 450°C/842°F is referred to as a *solder material*, or simply a “solder”; a filler metal with a liquidus temperature exceeding 450°C/842°F is a *brazing filler metal*. Although the distinction between the two processes is

determined solely by a melting property of the filler metals, the different temperature ranges have numerous attributes as well as drawbacks for the manufacturing processes that use either methodology. Some timely comparisons will be made throughout the text.

Lastly, it should be noted that the joining of two metals can also be realized by the use of adhesive materials, or “glues.” Generally, issues that need to be resolved with the use of adhesives are:

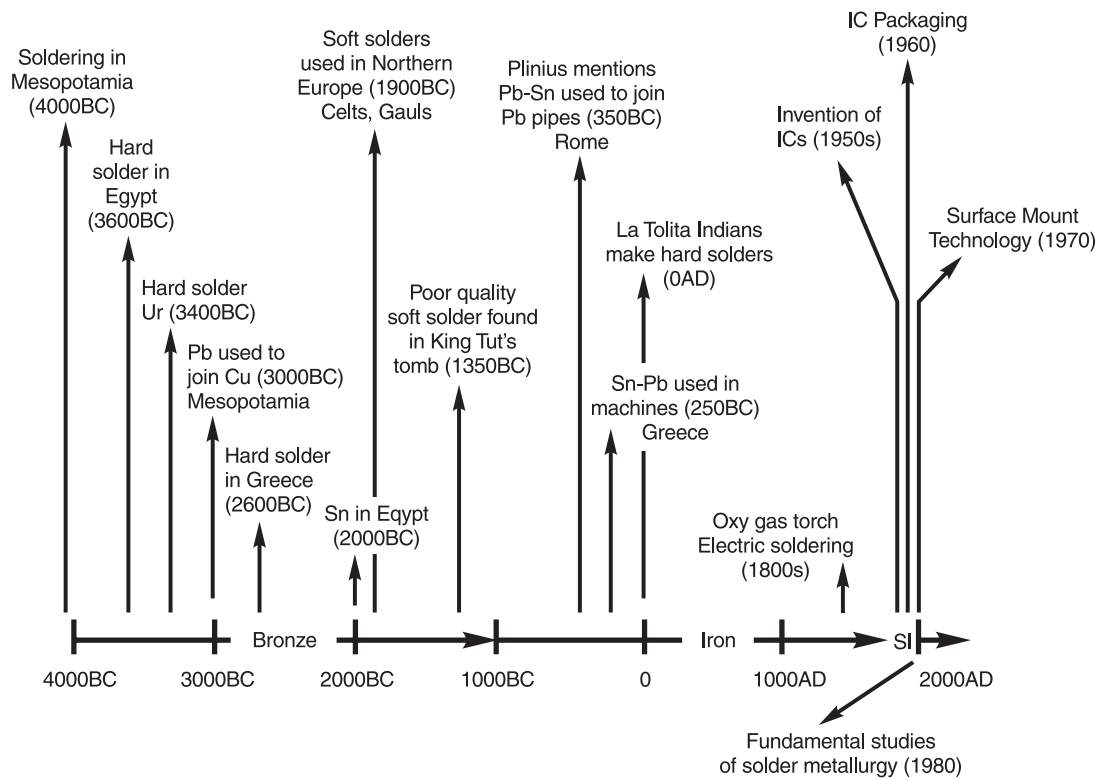
- (1) bulk strength levels to accommodate design loads;
- (2) adhesion strength; and
- (3) property stability (aging) over the service lifetime of the joint.

Although adhesives will certainly not replace the filler metal joining methodologies of brazing and soldering, they are finding many niche applications.

Soldering is a relatively old technology. Shown in Figure 1.1 is a time line which illustrates the 6000-year history of soldering [1]¹. Written details of the earliest uses of soldering are rare, since the art was generally practiced by slaves and considered unimportant to historians who, generally, belonged to society’s upper class. Archeological evidence of soldering from the earliest periods (4000 to 2000 BCE) is limited to artifacts, primarily jewelry and adornments, constructed with gold (Au)-based solders, since these materials were very resistant to corrosive deterioration. Artifacts having tin (Sn) based solders, the foundation of today’s soldering technology, are less prevalent, since Sn and Sn-based alloys more readily succumbed to corrosion by rainwater and naturally occurring chemicals in the ground.

The earliest practices with nonprecious metal solders were evidenced through the use of pure lead (Pb) by the

1. The numbers in brackets correspond to those in the references in Annex E.



(Reprinted by permission, The Metallurgical Society, TMS. Journal of Metals, Vol. 45, No. 7, "Issues in the Replacement of Lead-Bearing Solders," P. Vianco and D. Frear, p. 14, Fig. 1.)

Figure 1.1—Historical time line of soldering technology.

Mesopotamians in c. 3000 BCE to join copper (Cu) pieces. Pure Pb has a melting temperature of 327°C/621°F. Tin was not readily available to the Mediterranean cultures at that time. Tin and Sn-Pb solders were developed by the Celtic and Gaul cultures of Northern Europe in c. 1900 BCE, owing to the rich Sn ore deposits of that region. At that time, Sn-Pb solders were used to assemble tools and cooking utensils that were made largely of Cu and Cu-based alloys. The Romans used Sn-Pb solders to seal the Pb liners of their aqueducts.

As with the rest of Western Civilization during the Middle Ages, soldering experienced little progress, being limited to the making of jewelry and common household implements. However, the Industrial Revolution quickly expanded the use of soldering technology, particularly with the availability of portable heat sources, i.e., compressed gas for torches and electricity for the resistive heaters in soldering irons. Plumbing, including conduit and radiators, food and water containers, as well as light-duty tools and sheet-metal construction for automobile fenders and panels were some of the many uses to which soldering was applied. However, it was the advent of electronics in the early 20th century, and its continuing

evolution to the present day, which has quickly become the hallmark application of soldering technology.

Today, soldering technology can be categorized into two general fields based upon application:

- (1) *electronics soldering*, which describes the assembly of silicon microchip devices, printed circuit boards, motherboards, and connectors for the purpose of electrical signal transmission; and
- (2) *structural soldering*, which pertains to the role that is primarily that of mechanical fastening, i.e., non-electronic applications.

Clearly, many of the advances in soldering technology over the past half-century, both in the development of materials as well as new processes, have taken place in the electronics arena. However, these new materials and processes as well as an enhanced understanding of electronic solder joint properties can be applied equally to structural soldering applications. Failure to incorporate this increased understanding of solder joint behavior into larger scale, structural applications will only result in higher-than-necessary manufacturing costs, and an increased likelihood of poor product reliability. Irrespective of the source of innovation, all of soldering